Anisotropy and ageing effect on the mechanical behaviour of 3D-printed short carbon-fibre composite parts

L. Távara [a,*], C. Madrigal [b], M.T. Aranda [a], J. Justo [a]

[a] *Grupo de Elasticidad y Resistencia de Materiales, Escuela Técnica Superior de Ingeniería, Universidad de Sevilla, Camino de los Descubrimientos s/n, 41092 Sevilla, Spain*
[b] *Departamento de Ingeniería Mecánica y Fabricación, Escuela Técnica Superior de Ingeniería, Universidad de Sevilla, Camino de los Descubrimientos s/n, 41092 Sevilla, Spain*

ARTICLE INFO

ABSTRACT

The effect of ageing and anisotropy in 3D-printed composites including short carbon fibres embedded in a polyamide (PA/nylon®) matrix is analysed experimentally. A testing campaign including tensile and fracture toughness coupons with 100% infill is studied. The effect of anisotropy induced by the Fused Deposition Modelling (FDM) procedure, caused by the alignment of the fibres with the deposition direction (raster angle), is presented. Specifically, results showed that the Young modulus and the elastic limit values are lower for the +45/−45 infill configuration with respect to the 0/90 infill configuration. Conversely, the ultimate tensile strength, the ultimate tensile strain, and the fracture toughness values are higher for the +45/−45 infill configuration. Moreover, the crack path obtained in fracture toughness coupons always followed the raster angle. Additionally, experimental results show that the 3D-printed composite parts keep the hygrothermal properties associated to the matrix, thus an ageing effect is observed even for standard environmental conditions (room temperature, 50% relative humidity). Specifically, Young modulus, elastic limit and ultimate tensile strength values are lower for the older coupons. The ultimate tensile strain is higher for the older coupons while the fracture toughness is similar. Coupons stored in a desiccator also varied the properties but in a slightly manner.

1. Introduction

Additive Layer Manufacturing (ALM) is a well-established 3D-printing technique for prototyping, but its use for manufacturing structural parts is still an open matter. In this sense, a great effort has been done by the scientific community to manufacture parts with loading capacity using 3D-printed thermoplastics. The inclusion of (short or continuous) fibres within the polymeric matrix improves their mechanical properties, i.e. printing a composite material. Nowadays, Fused Deposition Modelling (FDM) is one of the most common techniques for printing composites. Among the different FDM possibilities, the use of a preimpregnated filament containing both the fibres and the resin is one of the most efficient option [1,2].

Previous works have shown that 3D-printed composites including continuous fibres are the best option for increasing the mechanical properties of thermoplastic resins [3]. Nevertheless, in parts with complex geometries (as those intended to be manufactured with 3D-printing) is not always feasible to include continuous fibre filaments, specially in zones where the raster angle tends to change abruptly (usually coinciding with zones that present stress raisers as corners, notches,

etc.) [4]. Thus, current ALM techniques use the base thermoplastic to fill in those zones. A way to alleviate this problem is to use short-fibre reinforced composites as the base thermoplastic. Thus, an adequate and accurate characterisation of this kind of composites is needed for a correct design of ALM parts.

Regarding the mechanical and physical characterisation of continuous fibre 3D printed composites, Justo et al. [3] analysed several properties of 3D printed composites, including continuous glass and carbon fibres (CFRP and GFRP, respectively), under tensile, compression and shear loading. Coupons were printed using the commercial 3D-printer MarkOne® [5], obtaining 50% fibre volume fraction for glass fibre composites and 40% fibre volume fraction for carbon fibre composites. A review including other mechanical properties under quasi-static conditions can be found in [6]. Fatigue and dynamic mechanical thermal analysis of 3D-printed CFRP can be found in [7], while notch sensitivity effect is presented in [8] and Dynamic Mechan-

---

* Corresponding author.
E-mail addresses: ltavara@us.es (L. Távara), cmadrigal@us.es (C. Madrigal), maranda@us.es (M.T. Aranda), jjusto@us.es (J. Justo).

ical Analysis (DMA) in [9]. Moreover, impact damage performance is studied in [10].

Other works focused on the analysis of fracture properties of 3D printed parts and the design of adhesive joints between these parts. In [11], the carbon fibre reinforced filament capabilities associated to the deposition path on V-notch and Open-Hole specimens are analysed numerically. Some strategies designed to improve the adhesive joint performance between 3D-printed CFRP laminates are described in [12]. Moreover, using the advantage of 3D-printing techniques, the design of structured interfaces is analysed in [13,14], results showed an increase of the fracture toughness of adhesive joints when structured interfaces are used. In [15], 3D-printed fasteners used in fastened and hybrid bonded/fastened joints are tested in single lap joint configurations. The feasibility of recycling and remanufacturing 3D-printed parts is studied in [16] by analysing the variations on the mechanical properties.

It is interesting to recall that in 3D-printed composites, the matrix is typically a thermoplastic, thus some intrinsic properties of this kind of polymers remain in the obtained composite. One effect that cannot be neglected is the ageing effect associated to the hygrothermal properties of the polymer. As an example, the effect of moisture on the impact behaviour of flax and basalt fibre reinforced composites is analysed in [17]. Moreover, a numerical model capable reproduce the impact behaviour of aged basalt fibre reinforced composites is presented in [18]. In addition, the effect of several moisture environments (ranging from 9 to 98% relative humidity) on the mechanical properties of 3D-printed continuous carbon and glass fibre reinforced composites is analysed in [19]. Results showed that moisture has a relevant effect on the properties. Similar results were shown in [20,21] for 3D-printed continuous carbon composites and in [22] for 3D-printed continuous glass fibre composites. Thermal ageing effects were also analysed in [23] for 3D-printed sandwich composites. In [24], the effect of carbon nanofibers (CNFs) content on hygrothermal ageing mechanisms of flax fibre-reinforced epoxy laminates is presented.

At the same time, it is well-known that the manufacturing process affects the material behaviour. Specifically, FDM (based on an injection procedure) introduces an anisotropic behaviour in 3D-printed parts, not only induced by the part orientation during layer deposition but also by the raster angle direction in the infill pattern. The latter effect is more clear when using continuous fibre reinforcement in 3D-printed composites. In [25], the strength of ABS parts manufactured by FDM under various loading conditions and printing directions is analysed. The fracture toughness of composites including cellulose fibres manufactured by injection moulding is studied in [26]. Results showed that the flow direction of the injection moulding process affects the orientation of the fibres. A crack analysis in transversely isotropic solids (i.e. short fibre reinforced polymer matrix composites) is presented in [27]. The analysis is based on stochastic modelling of statistical fluctuations of the transversal axis of fracture toughness. Furthermore, in [28], the influence of fibre orientation on extruded short carbon fibre PEEK composites under static and fatigue loading is presented.

Regarding the crack paths in anisotropic solids, specially with anisotropic fracture toughness, a deviation of the crack can be found, even for pure mode I loading condition. Analytical, numerical and experimental studies that analyse this effect can be found in the literature. For instance, a weak plane model is used in [29]. The model includes Extended Finite Element Models (XFEM) and a maximum energy release rate criterion. A different criterion that incorporates the T-stress concept and the interaction integral in a XFEM framework is presented in [30]. The deflection of mode I cracks is analysed experimentally in [31], and a model based on the J-integral and the maximum tangential stress criterion is also developed. Also, variational phase-field fracture is used together with a formulation of strain decomposition for crack growth analysis under tensile and compressive loads in [32].

Although the vast majority of 3D-printed composites research is focused on continuous fibre reinforcement, some works analyse the mechanical behaviour of 3D-printed short-fibre composites. Mechanical testing and SEM micrography of 3D-printed PLA including short carbon fibre reinforcement is presented in [33]. Results show that the presence of short fibres makes the printed material to behave in an orthotropic way, due to the short carbon fibres stay highly oriented with the material deposition direction. Several kinds of short fibres (fillers) embedded in a polypropylene matrix are analysed in [34]. In [35], the effect of short carbon fibres on PET and ABS matrix is studied. Results show that mechanical properties are enhanced when comparing to 3D-printed parts without reinforcements. The use of 3D-printed short carbon fibre laminates in sandwich structures is presented in [36]. Finally, a micromechanical model for predicting the non-linear elasto-plastic behaviour of short fibre reinforced composites is proposed in [37].

Consequently, the aim of the present research is to characterise the mechanical and fracture behaviour of 3D printed short carbon fibre composite parts. The filament used is called Onyx® and it is distributed by MarkForged® [5]. Special emphasis is taken on the anisotropic behaviour, inherent to the FDM process, as well as on the ageing effect over the obtained properties. It should be recalled that, on one hand, although some works analysed the anisotropic behaviour of 3D printed parts, until now, the use of "cross-ply" configurations is recommended in order to obtain a quasi isotropic behaviour. Nevertheless, even these kind of stacking sequences could present a highly anisotropic behaviour. On the other hand, the moisture effect was also studied but usually referred to extreme environmental conditions while the effect of moisture under standard environmental conditions was not analysed in detail. Therefore, the manuscript is organised in several sections, first, an analysis of the employed filament is presented. Then, the experimental campaign, including tensile and fracture toughness coupons, is described. Next, obtained results are introduced. Finally, a discussion on the anisotropy and ageing effects is presented.

2. Onyx filament analysis

The FDM system used in the present research is the MarkTwo® 3D-printer. It is able to print several kinds of filaments including continuous fibre reinforced nylon and a filament called Onyx®, which is composed of short carbon fibres embedded in nylon. The aim of the present section is to analyse some basic aspects of Onyx, as it is the filament chosen to manufacture every coupon in the present research.

2.1. Fibre percentage in weight

One of the key parameters in composite materials is the amount of fibres within the matrix. A way to measure this variable is to determine the fibre percentage in weight. For this purpose, three Onyx samples (portions of a filament) of raw material (before printing) were weighted. Then, a calcination procedure was done at 650 °C in an electric furnace. During the calcination, the nylon matrix is volatilised and only the fibres remain. As a result, the fibres form a kind of "dust" that was also weighted. Results showed an approximated 12.8% carbon fibre weight. Weighting was done in an electronic balance with ±0.1 mg precision.

2.2. Microscopic observation of the filament and fibres

An optical microscope was used to analyse the onyx filaments before printing and the short fibres after the calcination procedure.

In Fig. 1, micrographs of an Onyx filament section oriented perpendicular to the camera, inclined ~45° and oriented horizontally are presented, with 2.5× and 50× magnification. The pictures show that the short carbon fibres included in the onyx filament are already aligned following the axial direction of the filament. This fact is due to the manufacturing process of the filament, that entails an extrusion process. The alignment of the fibres can somewhat be seen in the inclined filament, Fig. 1(d), as the fibre sections seem to be slightly bigger than
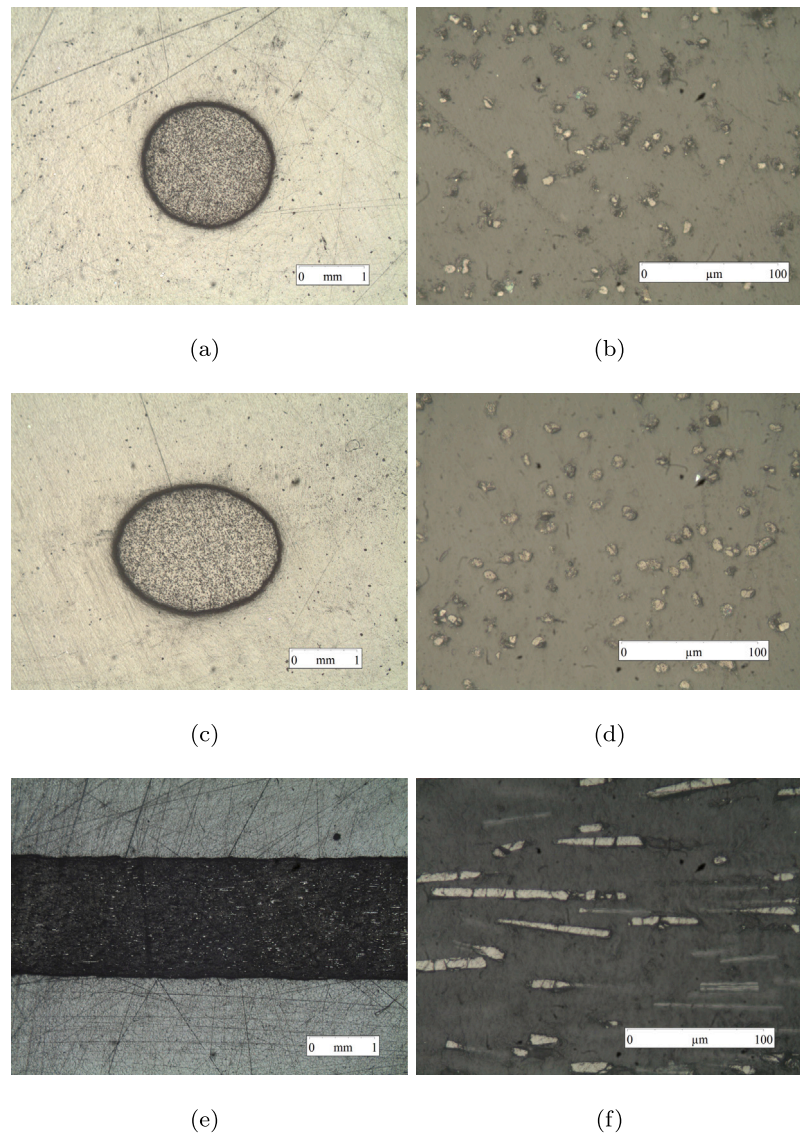
Fig. 1. Micrographs of an onyx filament section oriented perpendicular to the camera with magnification (a) 2.5× and (b) 50×; inclined ~45° with magnification (c) 2.5× and (d) 50×; and oriented horizontally with magnification (e) 2.5 and (f) 50×.

in Fig. 1(b). This is due to the visible fibre sections are cut in an inclined plane. In Fig. 1(f), the alignment can be clearly observed as several fibres are oriented almost horizontally. It is also interesting to notice from Fig. 1(b), that the short fibres do not have a circular section, as it is the case of continuous carbon fibres included in classical composites.

In Fig. 2, the fibres within an Onyx filament after the calcination process are shown. It can be observed that there is a great variability on the fibres length. Moreover, it can be seen that the short fibres are prisms with a variable section with non regular area, see Figs. 2(c) and (d), as mentioned previously. Considering that the sections can be represented by an ellipse, the mean major axis is around 7.4 µm.

Several pictures with 10x magnification were used to measure the length of the short fibres. The pictures were processed using a Matlab script that determines the length of each individual fibre. In Fig. 3, an example of this methodology is shown.

A total number of 1259 fibres were measured. The minimum, mean and maximum length obtained were 6.41 µm, 62.88 µm and 246.16 µm respectively. In Fig. 4, the distribution of the measured lengths is shown. It can be seen that more than 50% of the fibre lengths are within the range 29 µm–70 µm. It is also remarkable the great amount of very short fibres with less than 29 µm, while there is a very low number of fibres larger than 111 µm.

3. Tests and coupons description

In order to achieve the aim of the present research (to study the effect of anisotropy and ageing on the mechanical and fracture properties), two classical test configurations were analysed: the tensile test and the fracture toughness test.

The coupons were manufactured using a 100% infill. It is interesting to recall that 3D printing recommendations (regarding the infill pattern) suggest the use of cross-ply patterns to avoid the formation of pores that appear when a parallel pattern is used [1]. Moreover, MarkTwo® printer only allows the use of +45°/−45° infill patterns (aligned to the printing bed) when 100% Onyx infill is required. It is worth noticing that when a more complex geometry is printed, the +45°/−45° infill could work under different loading directions. For this reason, it is relevant to analyse the effect of the infill pattern on the global anisotropic behaviour of a printed part. In the present research two different infill patterns are used: +45°/−45° and 0°/90°. In order to get printed parts with a 0°/90° infill pattern, the part is rotated 45° with respect to the printing bed.

Thus, to analyse the ageing effect, four different configurations are studied considering the time passed from manufacturing to testing: 1

(a)

(b)

(c)

(d)
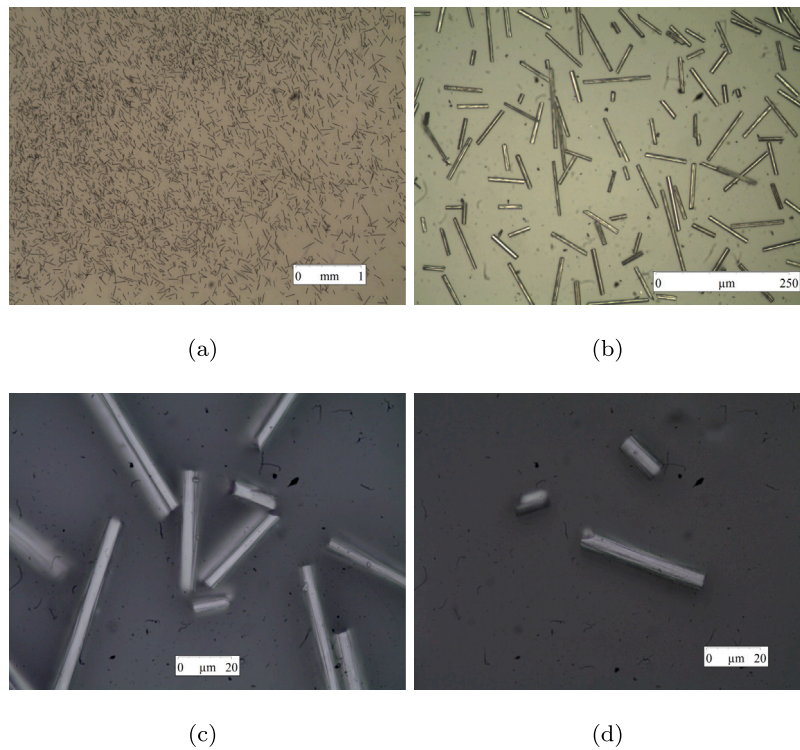
Fig. 2. Micrographs of the short fibres after calcination with magnification: (a) 2.5×, (b) 20×, (c) 100× and (d) 100×.
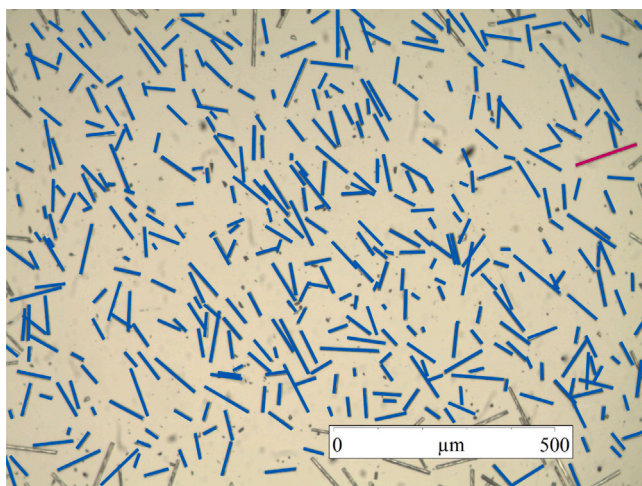
Fig. 3. Example of the method used to measure the short fibres length using a micrograph with 10× magnification.

Fig. 4. Distribution of the measured fibre lengths.

Table 1
Tensile coupon dimensions according to Fig. 5. L = 30 mm on the design and both printed coupons.

	Lo (mm)	Wo (mm)	W (mm)	t (mm)
Designed coupon	115	19	9	2
0/90 printed coupon	114.99	19.21	9.21	1.985
+45/−45 printed coupon	115.11	19.02	9.01	1.983

day, 30 days, 60 days and 60 days within a desiccator. The first 3 configurations were stored at standard environmental conditions (room temperature, 50% relative humidity). The latter option was selected as humidity could be a relevant factor when analysing the ageing effect, although some authors have established that other variables could also affect the material properties [22,24]. Every configuration has a margin of ±24 h.

3.1. Tensile test

Tensile tests are based on ISO 527 [38] and ASTM D638 [39] standards. The geometry of the manufactured coupon does not exactly follow none of these standards but it is very similar to type 1B included in [38] and type IV in [39]. The characteristic dimensions of the

designed coupon are shown in Fig. 5 and Table 1 together with those of the printed ones.

It is interesting to notice that most of the relevant dimensions are very similar for both printed configurations except by W and Wo. This difference is associated to the width of a printed filament, that is fixed to ~0.4 mm in the MarkTwo printer, which has direct impact on 0/90 printed coupons.

On the other hand, the thickness of each printed filament (and also of its corresponding layer) is 0.1 mm. Thus, each printed coupon has

(a)

(b)
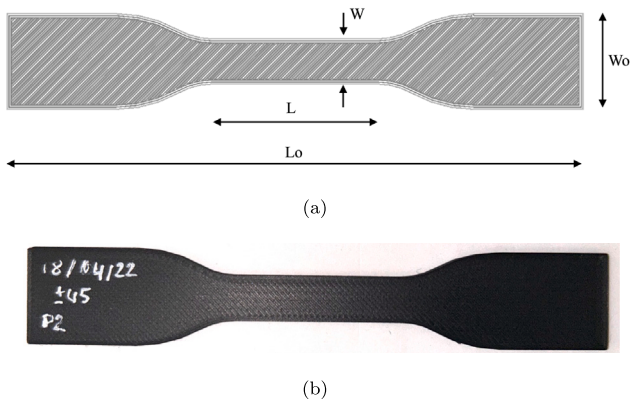
Fig. 5. (a) Tensile coupon designed geometry. (b) Picture of a finished sample.

(a)

(b)
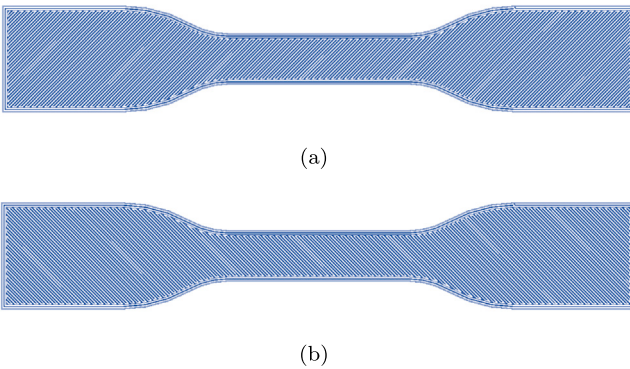
Fig. 6. Infill pattern obtained for a +45°/−45° tensile coupon.

20 layers. As mentioned previously, two infill patterns are analysed: 0/90 and +45/−45 configurations. In Fig. 6, the raster angle for even and odd layers for the +45/−45 configuration is shown. It should be noticed that two filaments are included along the border of each layer for a better surface finishing.

The coupons were tested on an Instron 4482 universal testing machine. The speed test was set to 0.5 mm/min and an extensometer with 25 mm gauge length was used.

3.2. Fracture toughness test

The plane strain fracture toughness tests carried out are based on ASTM D5045 [40] standard. The geometry of the manufactured coupons is the so-called Compact Tension (CT) configuration. The characteristic dimensions of the designed coupon are shown in Fig. 7 where the thickness is defined as 0.5 W and W being 40 mm in the present analysis.

In the present case, the characteristic dimensions of every printed coupon correspond to that of the designed coupon. Similarly to the tensile case, the thickness of each printed filament (and also of its corresponding layer) is 0.1 mm, and two filaments are included along the border of each layer. In CT configuration each printed coupon has 200 layers. Once again, two infill patterns are analysed: 0/90 and +45/−45 configurations. In Fig. 8, the raster angle for even and odd layers for the 0/90 configuration is shown.

Following the ASTM D5045 [40] standard, a natural crack at the notch was generated in every coupon using a fresh razor blade. The coupons were tested on an Instron 4482 universal testing machine. The speed test was set to 10 mm/min and a Crack Opening Displacement (COD) extensometer with 5 mm length gauge was used, although it is not required by the standard.

4. Test results

In the present section the results of the tensile and the fracture toughness tests are described. For each type of test, 3 coupons for each infill configuration (0/90 and +45/−45) and 4 ageing periods (1 day, 30 days, 60 days and 60 days in a desiccator) are presented.

4.1. Tensile test

In Fig. 9, the stress vs strain plots, obtained for every infill and ageing period configuration, are shown. Figs. 9(a), (c), (e) and (g) are associated to 0/90 infill for 1 day, 30 days, 60 days and 60 days in a desiccator, respectively. Figs. 9(b), (d), (f) and (h) are associated to +45/−45 infill for 1 day, 30 days, 60 days and 60 days in a desiccator, respectively.

It is remarkable that the mechanical behaviour in the tensile test is different for every analysed configuration. From these curves, it can be seen that maximum strain values for +45/−45 coupons are clearly larger than those for 0/90 coupons. Moreover, the maximum strain values also increase with the age of the coupons.

In Fig. 10, the summary of the Effective Young's Modulus obtained from the tensile tests is shown. Effective Young modulus is associated to the stiffness obtained for each configuration assuming the coupon is made of an homogeneous material. Results show that 0/90 configurations are stiffer than +45/−45 configurations. On the other hand, Young's modulus for older coupons are smaller when they are under similar ambient conditions. For coupons stored in the desiccator the stiffness is also reduced but in a slightly manner compared to the coupons of the same age in ambient conditions.

In Fig. 11, the summary of the elastic limit, σ_e, obtained from the tensile tests is shown. σ_e is obtained by the intersection of the $\sigma - \varepsilon$ plot and a line starting at $\varepsilon = 0.2\%$ with the slope of the initial part of the $\sigma - \varepsilon$ curve. Results show that +45/−45 configurations present a slightly lower strength than 0/90 configurations. On the other hand, σ_e for older coupons are smaller when they are under similar ambient conditions. For coupons stored in the desiccator the strength is also reduced but in a slightly manner compared to the coupons of the same age in ambient conditions.

In Fig. 12, the summary of the ultimate stress, σ_u, obtained from the tensile tests is shown. σ_u is the highest stress obtained during the test. Results show that +45/−45 configurations present a higher strength than 0/90 configurations. On the other hand, σ_u for older coupons are smaller when they are under similar ambient conditions. For coupons stored in the desiccator the strength is very similar compared to 1 day old coupons.

In Fig. 13, the summary of the ultimate strain, ε_u, obtained from the tensile tests is shown. ε_u is the strain obtained when σ_u is reached during the test. Results show that +45/−45 configurations present a higher ductility than 0/90 configurations. On the other hand, ε_u for older coupons are larger when they are under similar ambient conditions. For coupons stored in the desiccator the ductility is also increased but in a slightly manner compared to coupons of the same age in ambient conditions.

In Fig. 14, the fracture surface for the tensile coupons for every infill and ageing period configurations are presented. All the pictures have been taken with an inclination of 60° for an adequate observation of the fracture surface, that is, the transverse section of the coupons. Pictures in Figs. 14(a), (c), (e) and (g) are associated to 0/90 infill for 1 day, 30 days, 60 days and 60 days in a desiccator, respectively. While Pictures in Figs. 14(b), (d), (f) and (h) are associated to +45/−45 infill for 1 day, 30 days, 60 days and 60 days in a desiccator, respectively.

The fractographic analysis for the 0/90 coupons shows that the fracture plane is almost perpendicular to the applied load. The 1 day and 60 days in a desiccator coupons present the most planar fracture surface and the 0° and 90° plies can be easily distinguished. It is also interesting to notice that 30 and 60 days coupons present a
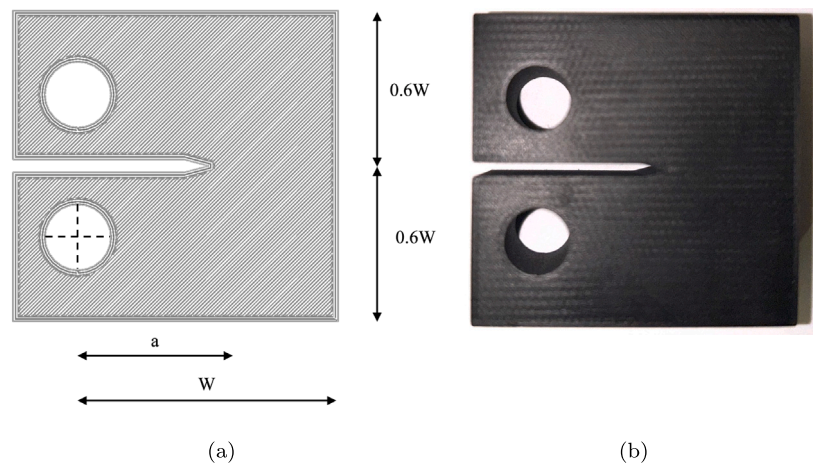
Fig. 7. (a) Compact Tension (CT) coupon designed geometry. (b) Picture of a finished sample.
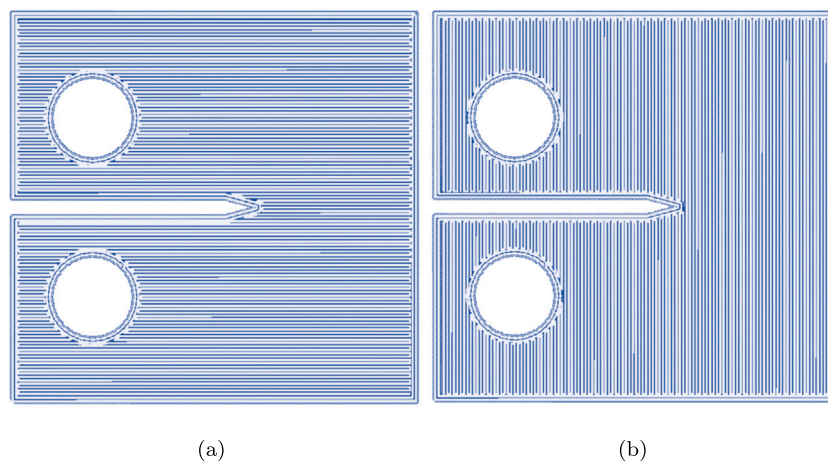
Fig. 8. Infill pattern obtained for a 0°/90° CT coupon.

concave zone in the central part of the fracture surface which could be associated with a larger plastic deformation. As a consequence, these coupons present larger values of maximum strain prior fracture.

Regarding the +45/−45 coupons, the fractographic analysis shows that the fracture plane is inclined with respect to the applied load, specially the 30 and 60 days coupons, which show larger plastic deformations. Moreover, It can be clearly seen that 60 days coupons present a necking phenomena which is associated to relevant plastic deformations.

4.2. Fracture toughness test

Although the standard ASTM D5045 [40] uses load vs displacement plots (both measured at the crosshead) to analyse the fracture toughness, in the present study the authors also used a crack opening displacement (COD) extensometer to analyse the CT specimens behaviour. The use of the COD allows to get a local measure on the crack tip vicinity and describes the fracture behaviour more accurately (i.e. linear or non-linear behaviour prior to the crack onset). It should be stated that the aim is to compare the fracture behaviour in Mode I of the different analysed configurations rather than obtaining the K_{Ic} values using the standard.

The standard uses P_Q or P_{max} for K_{Ic} calculation. Where P_Q is the load corresponding to the intersection of the load–displacement plot with a straight line with a slope of 95% of that of the initial part of the load–displacement curve, see Fig. 15(a). According to the standard, load vs. displacement plots should present a large linear part followed

by a short non-linear behaviour prior the crack propagation. Thus, P_Q and P_{max} should be similar. Nevertheless, in the present study, load vs displacement plots, obtained for every analysed configuration, show a large non-linear part, leading to large differences between P_Q and P_{max}. In Fig. 15, load vs crosshead displacement and load vs COD plots for a 0/90 infill 24 h coupon are shown. It can be seen that load vs COD plots do not allow to get the P_{max} value, as the COD extensometer is not able to capture large openings, but they may give a better approximation of P_Q value. In the present study, K_c^Q and K_c^{max} are defined as the fracture toughness obtained using P_Q and P_{max}, respectively, using equation (A2.1) in [40]:

$$K_c^Q = \frac{P_Q}{B\sqrt{W}}f(x), \qquad K_c^{max} = \frac{P_{max}}{B\sqrt{W}}f(x) \qquad (1)$$

being

$$f(x) = \frac{(2+x)(0.886 + 4.64x - 13.32x^2 + 14.72x^3 - 5.6x^4)}{(1-x)^{\frac{3}{2}}} \qquad (2)$$

where B is the specimen thickness in cm, W is the specimen width in cm, a the crack length in cm and $x = a/W$.

In Fig. 16, the summary of K_c^Q values is shown. Results show that +45/−45 configurations present a higher fracture toughness than 0/90 configurations. On the other hand, K_c^Q for older coupons are smaller when they are under similar ambient conditions. It is interesting to notice that coupons stored in the desiccator show the largest values of fracture toughness.
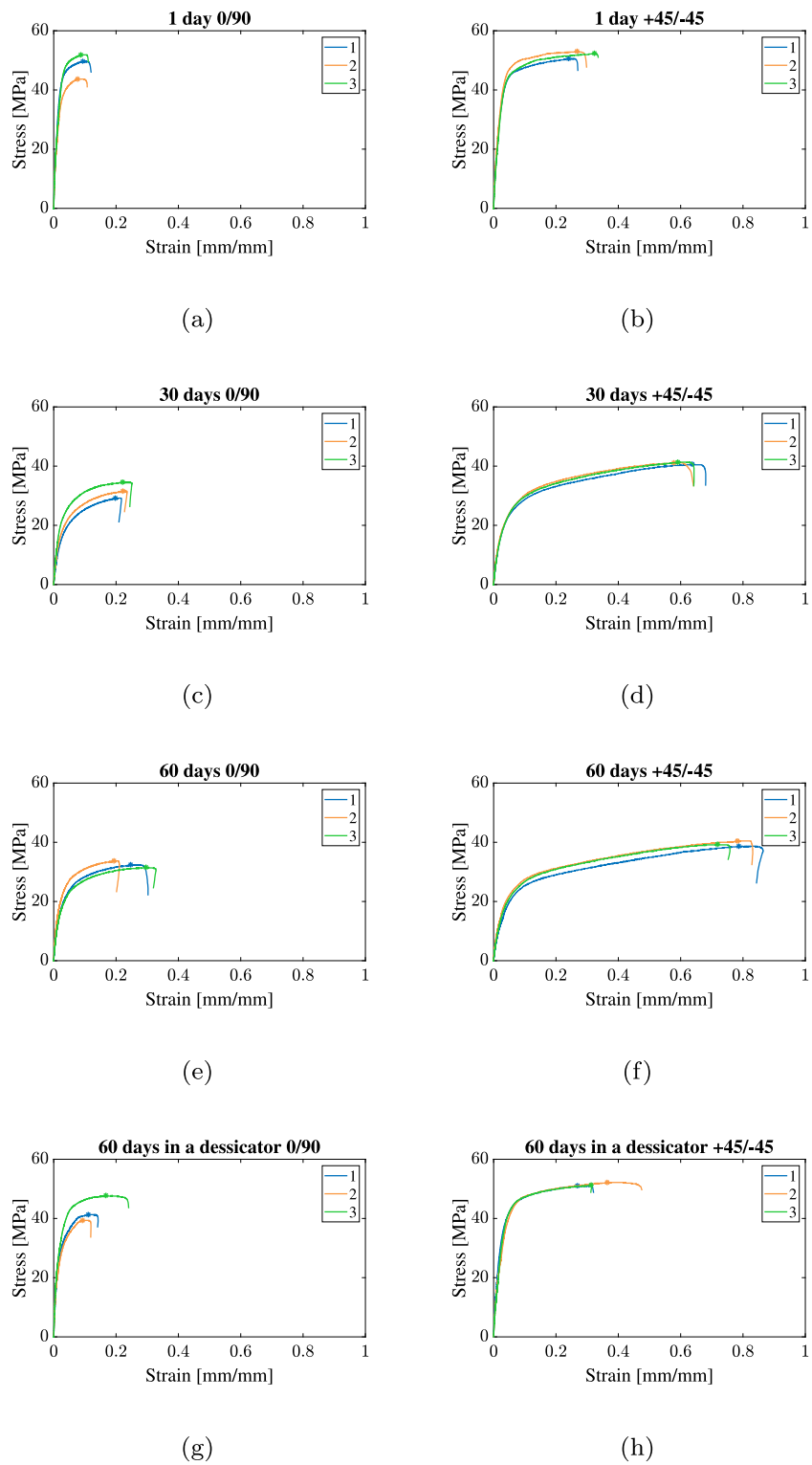
Fig. 9. Stress vs. strain plots obtained from the tensile test for (a) 0/90 infill 1 day, (b) +45/−45 infill 1 day, (c) 0/90 infill 30 days, (d) +45/−45 infill 30 days, (e) 0/90 infill 60 days, (f) +45/−45 infill 60 days, (g) 0/90 infill 60 days in desiccator, (h) +45/−45 infill 60 days in desiccator.

In Fig. 17, the summary of K_c^{max} values is shown. Results show that 0/90 configurations present a higher fracture toughness than +45/−45 configurations. On the other hand, K_c^{max} for older coupons are slightly smaller when they are under similar ambient conditions. Once again, coupons stored in the desiccator show the largest values of fracture toughness.

In Fig. 18, the crack path for both 0/90 and +45/−45 configurations is shown. It is also interesting to notice that the crack path is highly affected by the infill pattern. The crack grows perpendicular to the applied load in all coupons with 0/90 configuration (as expected in a CT test). On the other hand, the crack grows at 45° in all coupons with +45/−45 configuration.
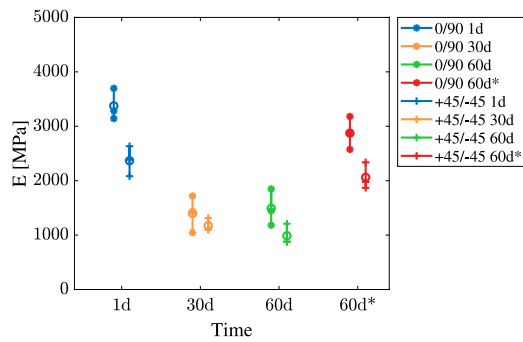
Fig. 10. Effective Young's Modulus, E, obtained from the tensile tests.
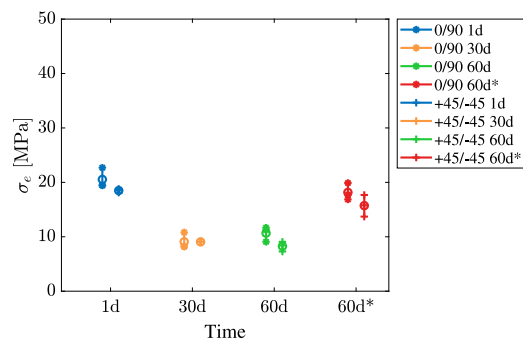
Fig. 11. Elastic limit, σ_e, obtained from the tensile test.
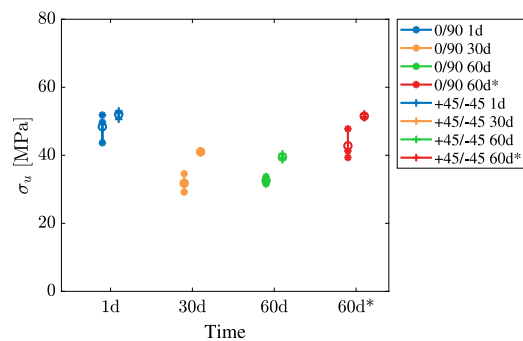
Fig. 12. Ultimate tensile strength, σ_u, obtained from the tensile tests.
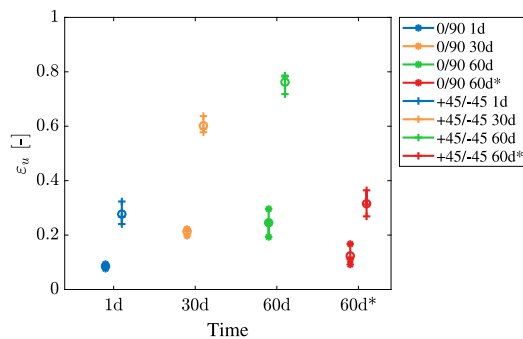
Fig. 13. Ultimate tensile strain, ε_u, obtained from the tensile test.

Regarding the fractographic analysis of CT coupons, the obtained fracture surfaces are very similar for every analysed configuration, as they are designed to behave in a brittle manner.

Table 2
Summary of the mean values of the measured mechanical and fracture properties.

Property	0/90 configuration				+45/−45 configuration			
	1d	30d	60d	60d*	1d	30d	60d	60d*
E [GPa]	3.37	1.40	1.49	2.87	2.37	1.17	0.99	2.06
σ_e [MPa]	20.53	9.08	10.66	18.16	18.49	9.06	8.25	15.72
σ_U [MPa]	48.41	31.77	32.57	42.80	52.01	41.04	39.49	51.50
ε_U [−]	0.086	0.214	0.245	0.123	0.277	0.602	0.762	0.315
K_c^Q [MPa$\sqrt{m}$]	1.15	0.93	0.93	1.49	1.26	1.09	0.91	1.36
K_c^{max} [MPa$\sqrt{m}$]	4.39	4.38	4.46	4.80	4.32	4.27	4.21	4.67

5. Discussion

Table 2 summarises the mean values of the measured mechanical and fracture properties. The experimental campaign shows that anisotropy (infill pattern) and the ageing period has a great impact on the properties of the 3D printed coupons.

5.1. Anisotropy effect

Although a 100% infill and cross-ply patterns are used, the tests have shown that both infill pattern configurations exhibit a very different behaviour. This fact is caused by the presence of aligned fibres in the printed filaments.

Fig. 19 shows several micrographs of a printed coupon cross-section of 0/90 configuration. The layers with 0° orientation can be clearly identified as the fibres are seen as dots. On the other hand, fibres in the 90° layers are identified as horizontal lines. Additionally, in Fig. 19(a), the border of the coupon is presented, where the thickness of each layer can be observed, as well as the fact that the printed filaments along the border always follow the perimeter of the coupon (i.e. 0° layers in the cross-section). It is also interesting to notice the large size of the pores that can be found between two adjacent 0° printed filaments, see black zones in Fig. 19(b).

Regarding the effect, on the properties and comparing coupons with the same age:

- Effective Young modulus (E): +45/−45 configurations always present smaller values of the Young modulus (i.e. more compliant), ranging from 0.66 to 0.84 times the value of its corresponding 0/90 configuration.
- Elastic limit (σ_e): +45/−45 configurations usually present smaller values of the Elastic Limit, ranging from 0.77 to 0.9 times the value of its corresponding 0/90 configuration, except by one case where similar values are obtained.
- Ultimate tensile strength (σ_U): +45/−45 configurations always present larger values of σ_U, ranging from 1.07 to 1.29 times the value of its corresponding 0/90 configuration.
- Ultimate tensile strain (ε_U): +45/−45 configurations always present larger values of ε_U (i.e. more ductile), ranging from 2.55 to 3.24 times the value of its corresponding 0/90 configuration.
- Fracture toughness (K_c^Q or K_c^{max}): Both configurations present very similar values, varying the ratio between +45/−45 and 0/90 configurations from 0.91 to 1.17.

The fact that the +45/−45 coupons present better properties than 0/90 coupons is associated to the anisotropic properties of each deposited (printed) filament. In this sense, 3D printed short fibre composite parts behave in a similar way as classical composites. That is, 0° plies present the best mechanical properties as the fibres play a major role (due to their alignment with the loading direction). 90° plies have the worst mechanical properties (as their properties are mainly associated to the matrix). 45° ply properties lie somewhere in between, but closer to those of 0° plies. It should be noticed that, in +45/−45 coupons every ply contributes to the effective properties of the laminate. Meanwhile, in 0/90 coupons the effective properties are mainly associated to 0° plies (half of the total).
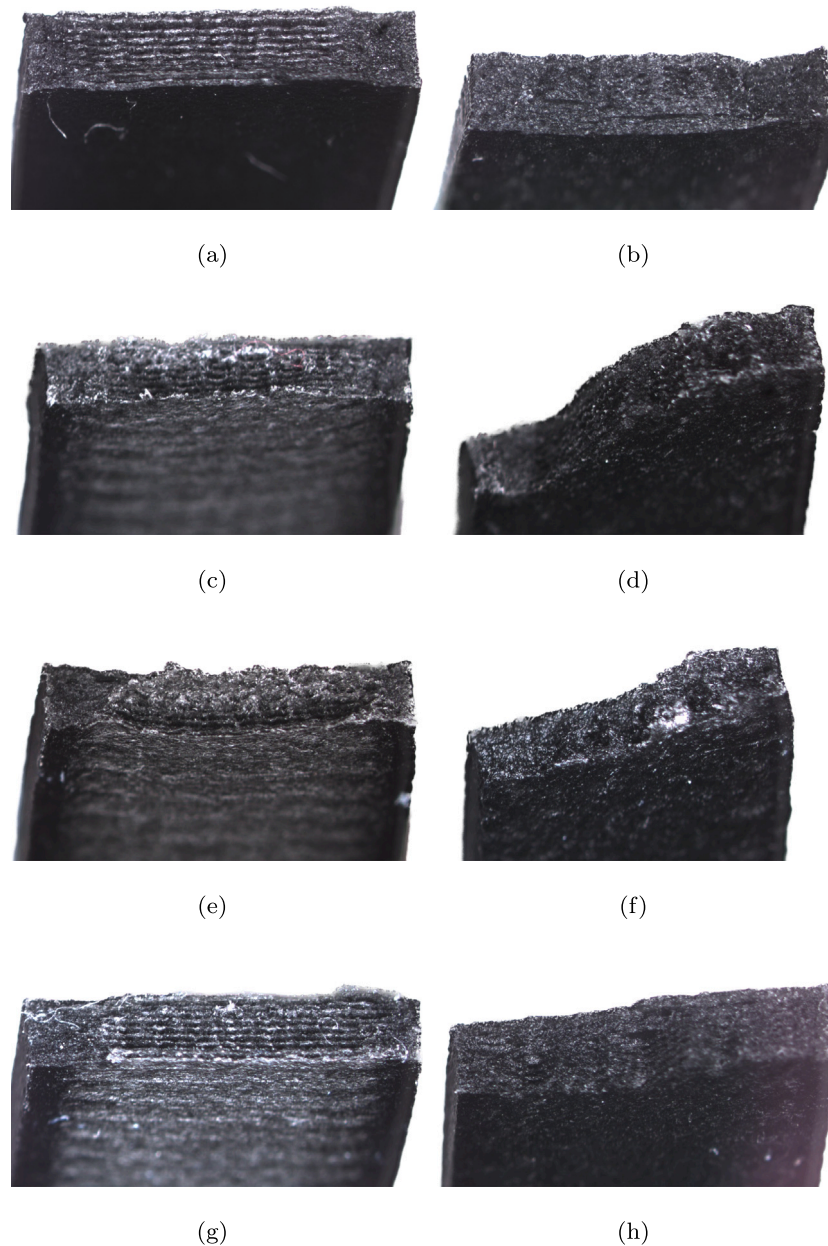
Fig. 14. Fracture surface for the tensile coupons with (a) 0/90 infill 1 day, (b) +45/−45 infill 1 day, (c) 0/90 infill 30 days, (d) +45/−45 infill 30 days, (e) 0/90 infill 60 days, (f) +45/−45 infill 60 days, (g) 0/90 infill 60 days in desiccator, (h) +45/−45 infill 60 days in desiccator.

5.2. Ageing effect

The results show that there is a relevant ageing effect on the mechanical and fracture behaviour. It was also proved that moisture takes an important role but it is not the only variable that affects the properties.

Regarding the effect on the properties (comparing the oldest to the fresh-printed coupons with the same infill configuration):

- Effective Young modulus (E): the oldest coupons (60 days) present smaller values of the Young modulus (i.e. more compliant), being 0.44 and 0.42 times the value of fresh-printed (1 day) coupons for the 0/90 and +45/−45 configurations under standard environmental conditions, respectively. The coupons stored in the desiccator during 60 days decreased E value in a slightly manner, being 0.85 and 0.87 times the value of fresh-printed coupons for the 0/90 and +45/−45 configurations, respectively.

- Elastic limit (σ_e): the oldest coupons present smaller values of the Elastic Limit, being 0.52 and 0.45 times the value of fresh-printed coupons for the 0/90 and +45/−45 configurations respectively under standard environmental conditions, respectively. The coupons stored in the desiccator during 60 days decreased the elastic limit value in a slightly manner, being 0.88 and 0.85 times the value of 1 day old coupons for the 0/90 and +45/−45 configurations, respectively.

- Ultimate tensile strength (σ_U): the oldest coupons present smaller values of σ_U, being 0.67 and 0.76 times the value of fresh-printed coupons for the 0/90 and +45/−45 configurations under standard environmental conditions, respectively. The coupons stored in the desiccator during 60 days decreased the ultimate tensile strength value in a slightly manner, being 0.88 and 0.99 times the value of fresh-printed coupons for the 0/90 and +45/−45 configurations, respectively.
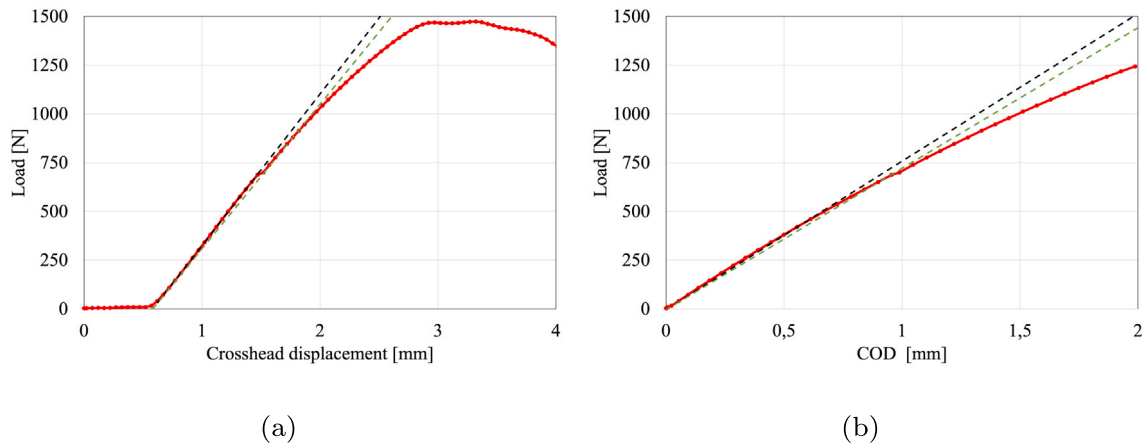
Fig. 15. (a) Load vs crosshead displacement and (b) Load vs COD plots for a 0/90 infill 1 day configuration.
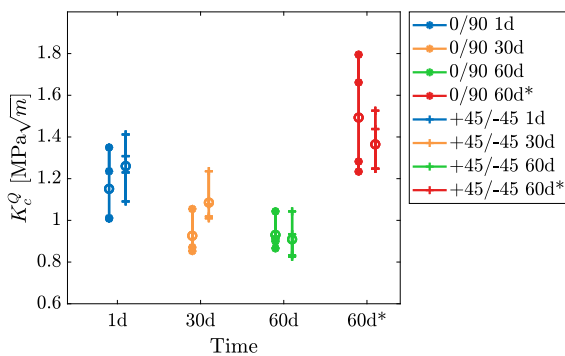
Fig. 16. Fracture toughness obtained using P_Q, see (1).
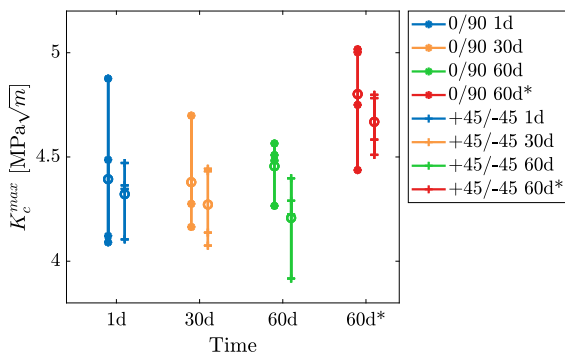
Fig. 17. Fracture toughness obtained using P_{max}, see (1).

- Ultimate tensile strain (ε_U): the oldest coupons present higher values of ε_U (i.e. more ductile), being 2.87 and 2.75 times the value of fresh-printed coupons for the 0/90 and +45/−45 configurations under standard environmental conditions, respectively. The coupons stored in the desiccator during 60 days increased the ultimate tensile strain value in a slightly manner, being 1.44 and 1.44 times the value of fresh-printed coupons for the 0/90 and +45/−45 configurations, respectively.
- Fracture toughness (K_c^Q): the oldest coupons present lower values of K_c^Q, being 0.81 and 0.72 times the value of fresh-printed coupons for the 0/90 and +45/−45 configurations under standard environmental conditions, respectively. On the other hand, the coupons stored in the desiccator during 60 days increased K_c^Q value, being 1.30 and 1.08 times the value of fresh-printed coupons for the 0/90 and +45/−45 configurations, respectively.

- Fracture toughness (K_c^{max}): Every configuration present very similar values. The oldest coupons present K_c^{max} values being 1.01 and 0.97 times the value of fresh-printed coupons for the 0/90 and +45/−45 configurations under standard environmental conditions, respectively. The coupons stored in the desiccator during 60 days increased the K_c^{max} value in a slightly manner, being 1.09 and 1.08 times the value of fresh-printed coupons for the 0/90 and +45/−45 configurations, respectively.

It should be highlighted the large differences between 60 days old coupons (stored or not in the desiccator). On the other hand, it is interesting to notice that fresh-printed coupons and 60 days in desiccator coupons present the best mechanical and fracture properties, with small differences between them. In view of these results, it can be concluded that moisture is one of the most relevant factors in ageing although it is not the only one affecting it.

6. Conclusions

In the present research a testing campaign is presented for 3D printed composite made of short carbon fibres embedded in a nylon® matrix (Onyx®). Tensile and fracture toughness tests for 100% infill coupons with two infill patterns and four ageing configurations were analysed. First, an analysis of the Onyx® filament used in the FDM procedure was done. A calcination procedure of the filament showed that they include 12.76% w/w of short carbon fibres, while a microscopic observation revealed that there is a great dispersion in the fibre lengths, being 6.4 μm, 62.9 μm, and 246.2 μm the minimum, mean and maximum observed lengths, respectively.

Testing results showed that there is an anisotropy effect induced by the raster angle, even for quasi isotropic configurations ("cross-ply" stacking sequences). Microscopic observations supported these conclusions, as they showed that short fibres are highly aligned with the deposition path. Moreover, all analysed mechanical and fracture properties were affected by the infill pattern. In particular, results showed that coupons with a +45/−45 infill pattern are more compliant, ductile and resistant than 0/90 infill pattern coupons. Moreover, in fracture toughness coupons, the crack path always followed the raster angle.

Experimental results also showed that 3D printed coupons present an ageing effect. Under standard environmental conditions the older coupons presented lower values of stiffness and strength, but a much higher ductile behaviour. Although moisture is an important factor on the ageing effect, it is clear that it is not the only factor associated to ageing. This fact can be confirmed as results showed that older coupons stored in a desiccator also changed their behaviour (but in a slightly manner).
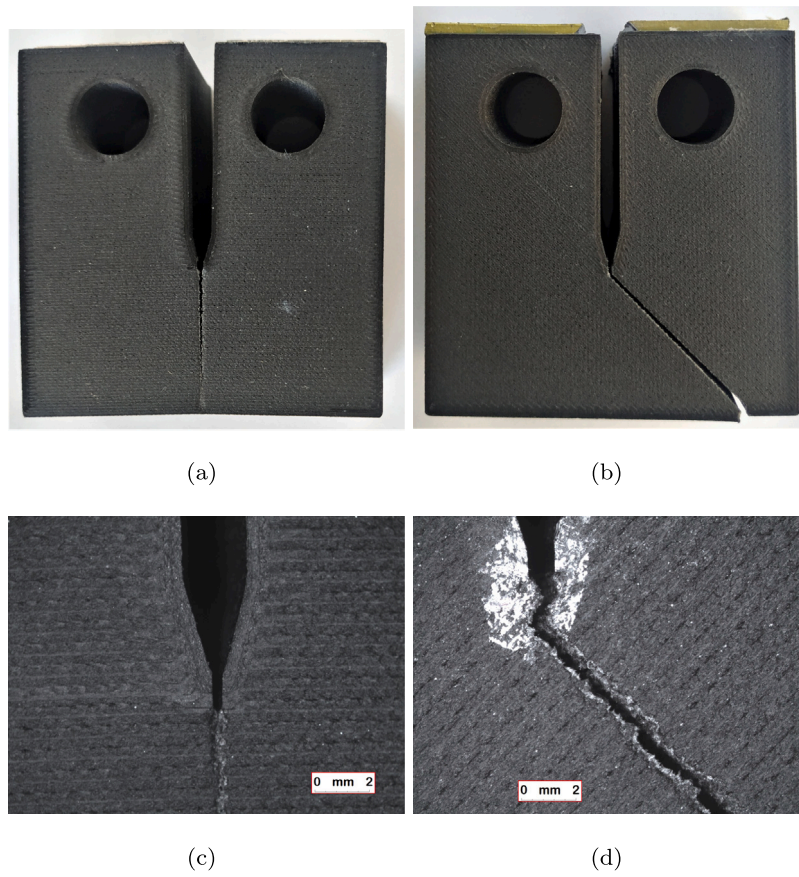
Fig. 18. (a) CT coupon with 0/90 configuration. (b) CT coupon with +45/−45 configuration. (c) Detail of the crack growth on a 0/90 configuration. (d) Detail of the crack growth on a +45/−45 configuration.
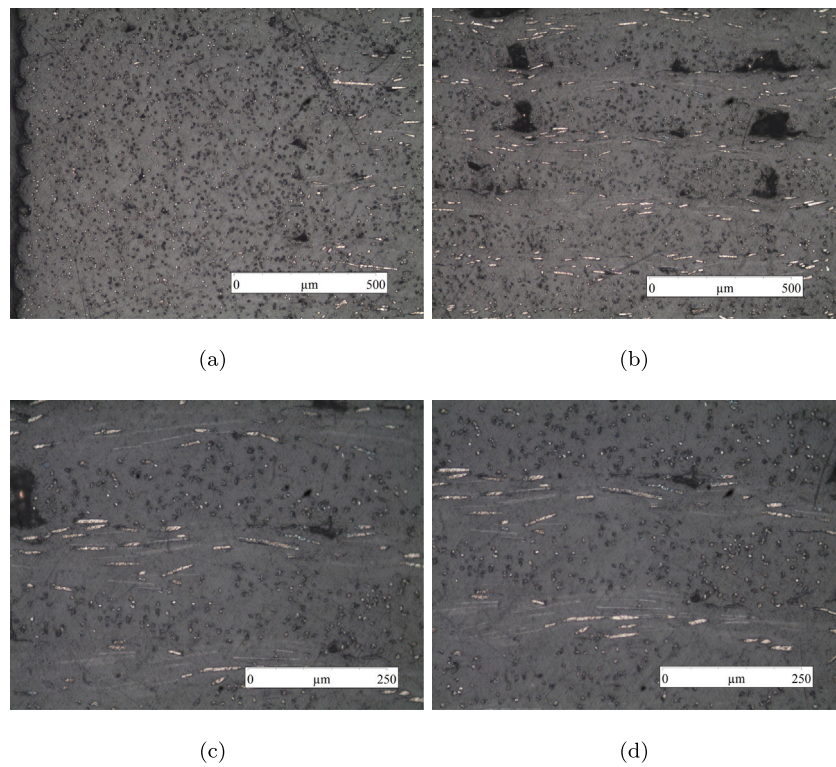
Fig. 19. Printed coupon with 0/90 configuration (a)10× zoom in a zone close to the border (b) 10× zoom, (c) 20× zoom and (d) 20× zoom.

In addition, the fractographic analysis of the tensile coupons showed that the fracture surface is different for every analysed configuration. The fracture surfaces of coupons with higher ductile behaviour presented larger plastic deformations.

For all these reasons, from a design point of view, it is relevant to take into account that 3D printed Onyx® parts present a relevant anisotropic behaviour and ageing effect (even for quasi isotropic configurations and standard environmental conditions) as shown in the present research.

CRediT authorship contribution statement

L. Távara: Conceptualization, Data curation, Formal analysis, Funding acquisition, Investigation, Methodology, Resources, Software, Supervision, Validation, Writing – original draft, Writing – review & editing. **C. Madrigal:** Conceptualization, Data curation, Formal analysis, Funding acquisition, Investigation, Methodology, Resources, Software, Supervision, Validation, Writing – review & editing. **M.T. Aranda:** Funding acquisition, Investigation, Methodology, Resources, Software, Writing – review & editing. **J. Justo:** Funding acquisition, Investigation, Methodology, Resources, Software, Writing – review & editing.

Declaration of competing interest

The authors declare that they have no known competing financial interests or personal relationships that could have appeared to influence the work reported in this paper.

Data availability

The raw data required to reproduce these findings are available to download from https://www.germus.es. The processed data required to reproduce these findings are available to download from https://www.germus.es.

Acknowledgements

References

[1] Rajan K, Samykano M, Kadirgama K, et al. Fused deposition modeling: process, materials, parameters, properties, and applications. Int J Adv Manuf Technol 2022;120:1531–70.

[2] Jiahui L, Yvonne D, Xiaodong H, Guangyong S, Dong R. Additively manufactured fiber-reinforced composites: A review of mechanical behavior and opportunities. J Mater Sci Technol 2022;119:219–44.

[3] Justo J, Távara L, García-Guzmán L, París F. Characterization of 3D printed long fibre reinforced composites. Compos Struct 2018;185:537–48.

[4] Plocher J, Wiol J-B, Panesar AS. Additive manufacturing with fibre–reinforcement - design guidelines and investigation into the influence of infill patterns. Rapid Prototyp J 2022;28(1241):7–1259.

[5] https://markforged.com. [Accessed 21 November 2022].

[6] Díaz-Rodríguez JG, Pertúz-Comas AD, González-Estrada OA. Mechanical properties for long fibre reinforced fused deposition manufactured composites. Composites B 2021;211:108657.

[7] Bendine K, Gibhardt D, Fiedler B, Backs A. Experimental characterization and mechanical behavior of 3D printed CFRP. Eur J Mech A Solids 2022;94:104587.

[8] Zhuang Y, Zou B, Ding S, Wang P. Shear and tensile behaviors of fiber-reinforced resin matrix composites printed by the FDM technology. Coatings 2022;12:1000.

[9] Alarifi IM. Investigation of the dynamic mechanical analysis and mechanical response of 3D printed nylon carbon fiber composites with different build orientation. Polym Compos 2022;43(8):5353–63.

[10] Caminero MA, Chacón JM, García-Moreno I, Rodríguez GP. Impact damage resistance of 3D printed continuous fibre reinforced thermoplastic composites using fused deposition modelling. Composites B 2018;148:93–103.

[11] Sangaletti S, García IG. Fracture tailoring in 3D printed continuous fibre composite materials using the phase field approach for fracture. Compos Struct 2022;300:116127.

[12] Pizzorni M, Lertora E, Parmiggiani A. Adhesive bonding of 3D-printed short- and continuous-carbon-fiber composites: An experimental analysis of design methods to improve joint strength. Composites B 2022;230:109539.

[13] García-Guzmán L, Távara L, Reinoso J, Justo J, París F. Fracture resistance of 3D printed adhesively bonded DCB composite specimens using structured interfaces: Experimental and theoretical study. Compos Struct 2018;188:173–84.

[14] Aranda MT, Reinoso J, García IG. On different 3D printing methods and fracture performance in DCB composite specimens including structured interfaces. Theor Appl Fract Mech 2022;122:103552.

[15] Li W, Guo S, Giannopoulos IK, Lin M, Xiong Y, Liu Y, et al. 3D-printed thermoplastic composite fasteners for single lap joint reinforcement. Compos Struct 2022;282:115085.

[16] Wei W, Chen L, Zhang L, Yang J, Yao Y, Zhang H. An experimental study on the properties changing in recyclable fiber-reinforced 3D printing. Polym Compos 2022;43(10):7187–99.

[17] Zivkovic I, Fragassa C, Pavlovic A, Brugo T. Influence of moisture absorption on the impact properties of flax, basalt and hybrid flax/basalt fiber reinforced green composites. Compos B Eng 2017;111:148–64.

[18] de Camargo FV, Pavlovic A, Schenal EC, Fragassa C. Explicit Stacked-shell modelling of aged basalt fiber reinforced composites to low-velocity impact. Compos Struct 2021;256:113017.

[19] Chabaud G, Castro M, Denoual C, Le Duigou A. Hygromechanical properties of 3D printed continuous carbon and glass fibre reinforced polyamide composite for outdoor structural applications. Addit Manuf 2019;26:94–105.

[20] Kikuchi BC, Bussamra FLS, Donadon MV, Ferreira RTL, Sales RCM. Moisture effect on the mechanical properties of additively manufactured continuous carbon fiber-reinforced Nylon-based thermoplastic. Polym Compos 2020;41:5227–45.

[21] Pizzorni M, Prato M. Effects of hygrothermal aging on the tensile and bonding performance of consolidated 3D printed polyamide-6 composites reinforced with short and multidirectional continuous carbon fibers. Composites A 2022;165:107334.

[22] Wang K, Chen Y, Long H, Baghani M, Rao Y, Peng Y. Hygrothermal aging effects on the mechanical properties of 3D printed composites with different stacking sequence of continuous glass fiber layers. Polym Test 2021;100:107242.

[23] Khosravani MR, Zolfagharian A, Jennings M, Reinicke T. Structural performance of 3D-printed composites under various loads and environmental conditions. Polym Test 2020;91:106770.

[24] Wang Y, Zhu W, Wan B, Meng Z, Han B. Hygrothermal ageing behavior and mechanism of carbon nanofibers modified flax fiber-reinforced epoxy laminates. Composites A 2021;140:106142.

[25] Górski F, Wichniarek R, Kuczko W, Zawadzki P, Buń P. Strength of ABS parts produced by fused deposition modelling technology – A critical orientation problem. Adv Sci Technol Res J 2015;9:12–9.

[26] Zarges JC, Minkley D, Feldmann M, Heim H-P. Fracture toughness of injection molded, man-made cellulose fiber reinforced polypropylene. Compos A Appl Sci Manuf 2017;98:147–58.

[27] Ricoeur A, Lindner F, Zarjov K. Stochastic aspects of crack deflection and crack path prediction in short fiber reinforced polymer matrix composites. Eur J Mech A Solids 2022;95:104598.

[28] Avanzini A, Battini D, Petrogalli C, Pandini S, Donzella G. Anisotropic behaviour of extruded short carbon fibre reinforced PEEK under static and fatigue loading. Appl Compos Mater 2022;29:1041–60.

[29] Gao Y, Liu Z, Zeng Q, Wang T, Zhuang Z, Hwang KC. Theoretical and numerical prediction of crack path in the material with anisotropic fracture toughness. Eng Fract Mech 2017;180:330–47.

[30] Mohtarami E, Baghbanan A, Hashemolhosseini H. Prediction of fracture trajectory in anisotropic rocks using modified maximum tangential stress criterion. Comput Geotech 2017;92:108–20.

[31] Judt PO, Zarges JC, Feldmann M, Ricoeur A, Heim HP. Deflecting mode-I cracks in anisotropic materials. Mech Mater 2019;136:103060.

[32] Luo Z, Chen L, Wang N, Li B. A phase-field fracture model for brittle anisotropic materials. Comput Mech 2022;70:931–43.

[33] Ferreira RTL, Amatte IC, Dutra TA, Bürger D. Experimental characterization and micrography of 3D printed PLA and PLA reinforced with short carbon fibers. Composites B 2017;124:88–100.

[34] Junaedi H, Baig M, Dawood A, Albahkali E, Almajid A. Mechanical and physical properties of short carbon fiber and nanofiller-reinforced polypropylene hybrid nanocomposites. Polymers 2020;12:2851.

[35] Tanabi H. Investigation of the shear properties of 3D printed short carbon fiber-reinforced thermoplastic composites. J Thermoplast Compos Mater 2022;35(2177):11–2193.

[36] Zaharia SM, Pop MA, Chicos LA, Buican GR, Lancea C, Pascariu IS, et al. Compression and bending properties of short carbon fiber reinforced polymers sandwich structures produced via fused filament fabrication process. Polymers 2022;14:2923.

[37] Mirkhalaf SM, van Beurden TJH, Ekh M, Larsson F, Fagerström M. An FE-based orientation averaging model for elasto-plastic behavior of short fiber composites. Int J Mech Sci 2022;219:107097.

[38] ISO. ISO-527-4. Part 4: Test conditions for isotropic and orthotropic fibre-reinforced plastic composites. 2021.

[39] ASTM. ASTM-D638-10, Standard Test Method for Tensile Properties of Plastics. 2010.

[40] ASTM. ASTM-D5045-14, Standard Test Methods for Plane-Strain Fracture Toughness and Strain Energy Release Rate of Plastic Materials. 2014.